Article

Chinese Science Bulletin

Polymer Chemistry

April 2012 Vol.57 No.10: 1109–1115
doi: 10.1007/s11434-011-4741-3

Spectroscopic investigation of the interactions between gold nanoparticles and bovine serum albumin

SHI XiuJuan[1], LI Dan[1,2], XIE Jing[1,2], WANG Shawn[3], WU ZhaoQiang[1] & CHEN Hong[1*]

[1] *College of Chemistry, Chemical Engineering and Material Science, Soochow University, Suzhou 215123, China;*
[2] *School of Material Science and Engineering, Wuhan University of Technology, Wuhan 430070, China;*
[3] *Department of Nanotechnology Engineering, University of Waterloo, Waterloo N2L3G1, Canada*

Received April 21, 2011; accepted May 31, 2011

The interactions between bovine serum albumin (BSA) and gold nanoparticles (AuNPs), and the conformational changes of BSA induced by this interaction, were investigated by UV-visible absorption spectroscopy, fluorescence spectroscopy, and Fourier transform infrared in combination with attenuated total reflection spectroscopy (ATR-FTIR). The critical adsorption density for preventing AuNP aggregation in 0.1 mol/L phosphate buffered saline (pH 7.2) was 23 BSA molecules per gold particle or 3.8×10^{12} BSA molecules/cm^2. BSA bound to the AuNPs with high affinity (binding constant $K_s=7.59\times10^8$ L/mol), and the intrinsic fluorescence of BSA was quenched by the AuNPs in accordance with the static quenching mechanism. Both fluorescence spectroscopy and ATR-FTIR showed that AuNPs induced conformational changes in BSA, which resulted in it becoming less compact and increased the polarity of the microenvironment around the tryptophan residue Trp-212.

AuNPs, BSA, stability, fluorescence, conformation

Citation: Shi X J, Li D, Xie J, et al. Spectroscopic investigation of the interactions between gold nanoparticles and bovine serum albumin. Chin Sci Bull, 2012, 57: 1109–1115, doi: 10.1007/s11434-011-4741-3

Gold nanoparticles (AuNPs) have many unique and attractive properties, such as excellent conductivity, size-dependant properties, optical properties, non-toxicity, and their capacity for facile and highly variable functionalization. They can easily form conjugates with proteins through either covalent bonds or physical interactions, and these conjugates have been widely applied in biomedical fields, including diagnostics, bio-imaging and targeted drug delivery [1–5]. Proteins have very complicated three dimensional structures with multi-level conformations, which are highly correlated with their biological activities and activation of the immune response [6], and interaction with nanoparticles can disturb these proteins structures to various extents. In turn, proteins may affect the optical properties of AuNPs, and their stability in solutions with high ionic strength [7–13]. To design an effective AuNPs-protein system for biological applications, it is necessary to study the AuNPs-protein interactions systematically. Some studies have investigated the influence of AuNP size on the conformation of cytochrome *c* [14]; and the effect of pH on the conformation of BSA adsorbed on the surface of AuNPs [15]. Fluorescence spectroscopy [11,16], dynamic light scattering [8,17], circular dichroism [9,18], Fourier transform infrared spectroscopy (FTIR) [19], nuclear magnetic resonance spectroscopy [20], surface enhanced Raman scattering [21], time-correlated single photon counting spectroscopy [13,22] are among a variety of techniques commonly used to characterize AuNPs-protein interactions. The combination of different techniques will give us insight into the interactions of AuNPs and proteins.

Bovine serum albumin (BSA) plays a significant role in many important physiological functions, and its structure and conformation can be easily changed [23]. AuNPs-BSA bioconjugates have been used in several applications such as intracellular delivery vectors and imaging agents [13]. Fundamental studies on the interactions between AuNPs and BSA may contribute to development of optimal condi-

*Corresponding author (email: hongchen@whut.edu.cn)

tions for forming bioconjugated nanomaterials that preserve the functionality of proteins. Recently, several studies on the AuNPs-BSA bioconjugates have been reported. Sen et al. [22] and Burt et al. [24] synthesized AuNPs directly conjugated to BSA by chemical reduction in aqueous solution. The conjugation of AuNPs-BSA occurred mainly through electrostatic interactions [11,15]. In addition, the binding constant for glutamic acid-AuNPs-BSA and a decrease in the α-helical content after conjugation were reported [18]. Shang et al. [15] showed that the conformational changes of BSA were larger at higher pH and a blue shift of the fluorescence emission maximum was observed after colloidal gold was added to the BSA solution. However, there are few reports of the specific interactions between citrate-coated AuNPs and BSA.

In this study, BSA was conjugated with AuNPs (13.9 nm) and the interactions between them were studied by UV-visible absorption (UV-Vis) spectroscopy, fluorescence spectroscopy and Fourier transform infrared in combination with the attenuated total reflection spectroscopy (ATR-FTIR). Based on the data obtained using these techniques, the effects of BSA concentration on the stability of the AuNPs and the conformational changes of BSA upon interacting with the AuNPs are discussed, and a possible mechanism of the conjugation is proposed.

1 Experimental

1.1 Materials

Chloroauric acid ($HAuCl_4 \cdot H_2O$) was purchased from Shanghai Chemicals Co. (Shanghai, China). BSA was obtained from Sigma-Aldrich (St Louis, MO), and a solution was prepared in 0.1 mol/L phosphate buffered solution (PBS, pH 7.2). Trisodium citrate ($Na_3C_6H_5O_7 \cdot 2H_2O$) was obtained from Lingfeng Chemicals Co. (Shanghai, China). All the reagents except for BSA were AR grade and used as received. The water used in the experiments was purified in a Milli-Q system (Millipore Co., Molsheim, France).

1.2 Preparation of AuNPs

All glassware used in the experiments was cleaned in freshly prepared aqua regia ($HCl:HNO_3$=3:1, v/v) and rinsed thoroughly with water prior to use. AuNPs were prepared following Frens' method [25]. An aqueous solution of $HAuCl_4$ (0.25 mmol/L, 20 mL) was heated to its boiling point while stirring vigorously, and then 0.2 mL of trisodium citrate solution (0.189 mol/L) was added quickly, which resulted in the solution changing color from pale yellow to deep red. This mixture was boiled for an additional 20 min and then cooled to room temperature by stirring. This colloidal gold had an average particle size of 13.9 nm and a polydispersity index of 0.222 as measured by laser particle size analyzer. The concentration of the AuNPs was calculated using an established method [26] to be approximately 3.0 nmol/L, assuming that all gold in the $HAuCl_4$ was reduced.

1.3 Preparation of AuNPs-BSA bioconjugates

The AuNPs-BSA bioconjugates were prepared by mixing the solution of BSA and AuNPs in PBS (0.1 mol/L, pH 7.2), then incubating the mixture at 277 K for at least 1 h in the wells of a microtitre plate. A series of bioconjugates with different amount-of-substance ratios of BSA/AuNPs were prepared by keeping the concentration of AuNPs (1.3 nmol/L) constant while varying the concentration of BSA from 0 to 152 nmol/L for the UV-Vis absorption spectra. For the fluorescence emission spectra, the BSA concentration was kept constant at 1 μmol/L while the AuNPs concentration was varied from 0 to 0.5 nmol/L. To prevent shear forces from disrupting the structure of the bioconjugates, no separation techniques (e.g., centrifugation or filtration) were used in the experiment. All the measurements were performed at room temperature (293 K).

1.4 Absorption spectra

The absorption spectra of different AuNPs-BSA conjugates were recorded from 400–700 nm with an interval of 2 nm using a 5 nm slit-width. Absorption blanks, water for the aqueous solution of AuNPs and PBS for the AuNPs-BSA conjugates, were subtracted from the absorption spectra of the relevant samples to correct the influence of the background.

1.5 Fluorescence measurements

The fluorescence emission spectra were recorded from 315 to 500 nm with an excitation wavelength of 295 nm and a 2 nm interval and 5 nm slit-width. Each spectrum is the average of three scans. PBS was used as a fluorescence emission blank and subtracted to correct the fluorescence background. Before analysis of the samples, it was confirmed that the AuNPs alone did not fluoresce on excitation at 295 nm.

1.6 ATR-FTIR measurements

The concentrations of BSA and AuNPs in the bioconjugates for the FTIR study were 3×10^{-4} and 2.5×10^{-9} mol/L, respectively. All the spectra of the bioconjugates were recorded via the ATR method with a resolution of 2 cm^{-1} from 4000 to 1000 cm^{-1}. A reference spectrum of the same solution without protein was recorded under identical conditions. Spectra of BSA in solution and of BSA interacting with AuNPs were obtained from corresponding difference spectra, which were smoothed slightly to eliminate the influence of the absorption from residual vaporized water.

Fourier self-deconvolution and secondary derivative analysis were applied to the spectrum from 1600–1700 cm^{-1}

with OMNIC 8.0 (Thermo Fisher Scientific, Waltham, MA) software to estimate the number, position and width of the component bands. Based on these parameters, a curve-fitting process was carried out to obtain the best Gaussian-shaped curves that fit the original protein spectrum. After indentifying individual bands with the representative secondary structure, the percentages of each secondary structure of BSA were calculated from the relative area of the component bands.

1.7 Instrumentation

The size of AuNPs was measured with a laser particle size analyzer, HPP5001 (Malvern Instruments, Malvern, UK). The optical absorption and fluorescence spectra were recorded on a Multiskan Spectrum Microplate Spectrophotometer (Varioskan Flash, Thermo Fisher Scientific). FTIR spectra were recorded on a Nicolet Magna 6700 FTIR spectrometer (Thermo Fisher Scientific) equipped with a germanium ATR accessory, a DTGS (Deuterated triglycine sulfate) KBr detector, and a KBr beam splitter.

2 Results and discussion

2.1 Effect of BSA concentration on the AuNPs stability

UV-Vis absorption spectroscopy is the most widely used method for characterizing the optical properties of AuNPs because the intensity and position of the surface plasmon band of colloidal gold are related to the size, shape and dispersity of the AuNPs. An aqueous solution of pure AuNPs showed a narrow and symmetric absorption peak at approximately 518 nm (curve h, Figure 1), which agreed with an earlier report [27]. This indicates the AuNPs are monodisperse and spherical [28]. A red shift and a broadening of the absorption band were observed in the presence of BSA. These changes indicate that BSA has adsorbed on the surface of AuNPs [17]. Although it may seem unusual that the negatively charged, citrate-coated AuNPs could adsorb onto BSA, which is also negatively charged overall at pH 7.2, BSA has 60 surface lysine residues that can be protonated and interact electrostatically with the negatively charged AuNPs [29]. Moreover, other forces such as hydrophobic interactions may also be involved in the conjugation of the protein with the AuNPs [30].

The absorption bands gradually shifted and widened as the BSA content in the mixture decreased. At a BSA concentration of 30 nmol/L, a new peak centered around 606 nm appeared (curve c, Figure 1), which signals the AuNPs have aggregated. The spectrum also shows a broad band centered around 662 nm in the absence of BSA (i.e., AuNPs in PBS, curve a, Figure 1), while the absorbance at 518 nm became weaker and blue-shifted. The aggregation is caused by the electrolytes in PBS, because of the shielding of the repulsive double-layer charges that normally stabilize the AuNPs

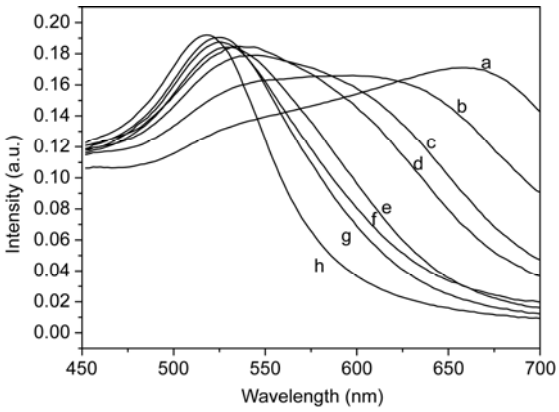

Figure 1 Absorption spectra of mixtures of 1.3 nmol/L AuNPs and BSA at concentrations of 0 (a), 15 (b), 30 (c), 38 (d), 61 (e), 121 (f) and 152 (g) nmol/L in 0.1 mol/L PBS (pH 7.2); and 1.3 nmol/L aqueous solution of AuNPs (h).

[14,17]. However, aggregation can be avoided if sufficient BSA is added to PBS. This may be attributed to the following reasons: firstly, BSA forms a protective layer on the AuNPs surface, and the colloidal suspensions could be stabilized by the interaction of protein side chains or domains, resulting in a reduction in entropy and a loss of solvation enthalpy, both of which keep the system stable [29]; secondly, BSA bound to the AuNPs surface is continuously exchanged with free BSA [20], which should also improve the stability of the AuNPs solution. Because AuNPs started to aggregate when the BSA concentration decreased to below 30 nmol/L, this roughly indicates the critical concentration of BSA to prevent AuNP aggregation. Therefore, 23 BSA molecules per gold particle (i.e., 3.8×10^{12} BSA molecules/cm^2) are required to prevent aggregation. At this concentration, BSA should be attached to the nanoparticle surfaces as a monolayer [14]. Xie et al. [13] reported that no more than 50 BSA molecules could be adsorbed to form a monolayer on a citrate stabilized AuNP with a particle size of 15 nm. This means that the amount of BSA required to stabilize AuNPs is less than the amount required to reach monolayer saturation for AuNPs.

2.2 Analysis of the AuNPs-BSA interactions

BSA have tryptophan (Trp), tyrosine (Tyr) and phenylalanine (Phe) residues, which can absorb and emit ultraviolet light. The fluorescence intensities of these residues decrease in the following order: Trp>Tyr>Phe [30]. Each BSA molecule has two Trp residues, one of which is located at the bottom of the hydrophobic pocket in domain II (Trp-212), while the other is in domain I (Trp-134) on the surface of the molecule [31–33]. Because the excited-state dipole moment of Trp is relatively large, the emission energy is highly sensitive to the polarity of the environment. Conformational changes in BSA may disturb the microenvironment around the Trp residues and thus influence the fluorescence

emission. Therefore, the Trp fluorescence is widely used to monitor conformational changes in proteins [31,34].

In this paper, Trp was used as the intrinsic fluorescence probe with excitation at λ=295 nm to monitor the fluorescence quenching of BSA by the AuNPs [34–36]. The fluorescence intensity of BSA gradually decreased as the AuNPs concentration increased (Figure 2(a)), which indicates that the AuNPs are responsible for quenching of the fluorescence [28]. When the binding site on the surface of the AuNPs is in close proximity to the Trp residues of BSA, the fluorescence from the Trp is quenched and the remaining fluorescence is from other free Trp residues in the solution. We suspect that the majority of these quenched Trp residues should be Trp-134, because it is present at the surface of BSA and therefore more likely to be positioned close to the surface of AuNPs in the conjugates.

The main quenching mechanism includes dynamic quenching and static quenching. The former results from the collision of quenchers and excited-state fluorophores, while the latter involves the formation of a nonluminous complex between quenchers and ground-state fluorophores [37,38]. The Stern-Volmer equation (eq. (1)) was used to determine the dominant quenching process in the AuNPs-BSA conjugate system.

$$\frac{F_0}{F}=1+k_q\tau_0[\mathrm{Au}]=1+K_{SV}[\mathrm{Au}]. \quad (1)$$

In this equation, F_0 and F are the relative fluorescence intensities in the absence and presence of AuNPs, respectively; [Au] is the concentration of AuNPs; k_q is the quenching rate constant; K_{SV} is the Stern-Volmer dynamic quenching constant, which is related to the bimolecular collision process; and τ_0 is the lifetime of a fluorophore in the absence of quenchers.

According to eq. (1) and the trend-line shown in the Stern-Volmer plot (Figure 2(b)), K_{SV} was calculated to be 7.64×10^8 L/mol, which indicates the AuNPs have a strong quenching ability. The intrinsic fluorescence of BSA is known to have $\tau_0=5\times10^{-9}$ s [15], and the k_q can be calculated at 1.53×10^{17} L/(mol s). This value is much greater than the maximum value for a diffusion-controlled quenching process (approximately 2.0×10^{10} L/(mol s) [19]), which suggests that the fluorescence quenching process of BSA in the presence of AuNPs is a static quenching process [35,39]. For the static quenching process, if the protein has the same and independent binding sites, the binding constant (K_s) and the number of binding sites (n) can be calculated based on the following equation [38,40]:

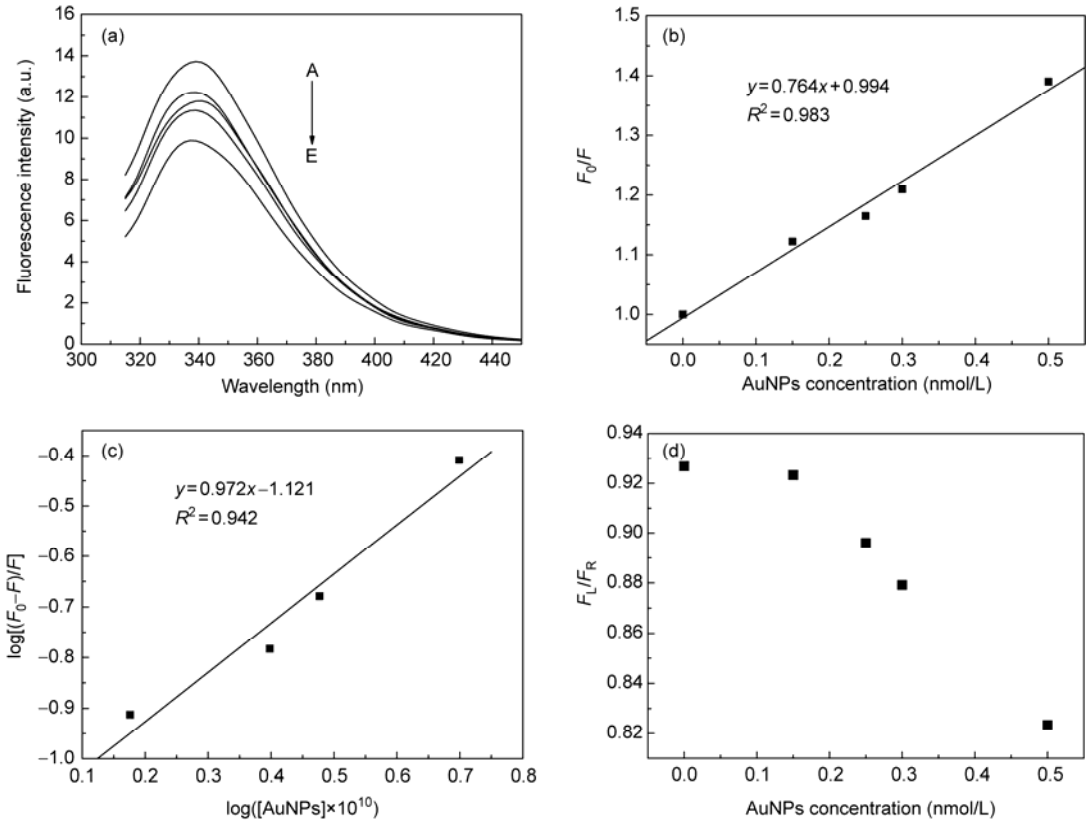

Figure 2 (a) Fluorescence emission spectra of BSA solutions (1 μmol/L) in the presence of AuNPs with the following concentrations: 0 (A), 0.15 (B), 0.25 (C), 0.3 (D), 0.5 (E) nmol/L; (b) the Stern-Volmer plot of BSA with an increasing concentration of AuNPs; (c) the plot of log[(F_0–F)/F] vs. log[AuNPs] for BSA conjugated with AuNPs; (d) position of the Trp emission maximum as a ratio of the fluorescence intensities 20 nm left (F_L) and right (F_R) of the emission maximum of curve A in Figure 2(a).

$$\log\left[\left(F_0 - F\right)/F\right] = \log K_s + n\log[\text{AuNPs}]. \quad (2)$$

Based on the experimental data, $\log[(F_0 - F)/F_0]$ was plotted against log[AuNPs] (Figure 2(c)), and the number of binding sites was calculated to be 0.972. This shows that n is almost equal to 1, and that the average number of independent classes of binding sites on BSA for AuNPs is 1 [38]. The binding constant (K_s) was calculated to be 7.59×10^8 L/mol, which is much greater than those of the binding of proteins with small molecules (typical range 10^3–10^6) [35,41].

To identify the changes in the emission peak of BSA in the presence of AuNPs in Figure 2, the parameters F_L and F_R were introduced. These parameters represent the fluorescence intensities at the wavelength 20 nm to the left (F_L) and right (F_R) of the emission maximum of curve A in Figure 2(a) at 339 nm [35]. By comparing the values of F_L/F_R calculated from the spectra, the direction the emission maximum shifted in could be determined. As shown in Figure 2(d), the value of F_L/F_R decreased as the concentration of AuNPs increased, which indicates that a red shift occurred. This suggests that the polarity of the microenvironment around the Trp residues increases because of the conformational changes of BSA at the tertiary structure level [15,35]. By contrast, Shang et al. [15] found that conjugation of BSA and AuNPs led to a blue shift in the fluorescence emission maximum. This blue shift was attributed to the proximity of the Trp residues to the hydrophobic surface of the AuNPs. However, Brewer et al. [29] suggested that BSA conjugates with citrate-coated AuNPs mainly through electrostatic interactions, rather than through direct binding to the surface of the bulk AuNPs. Herein, we suggest that the adsorption of BSA on the AuNPs forces the BSA molecules to transform into a less compact structure, which allows the solvent to penetrate into the hydrophobic cavity of BSA, which increases the polarity of the microenvironment around Trp-212. Therefore, the microenvironment changes around Trp-212 should be the main reason for the red shift of the fluorescence emission maximum that was observed.

2.3 Effects of AuNPs on the BSA secondary structures

ATR-FTIR spectroscopy was used to monitor the changes in the secondary structures of BSA upon interaction with the AuNPs. Amine I is the most sensitive probe for detecting changes in the protein secondary structures. Its characteristic absorption band is located at 1600–1700 cm^{-1}. By comparing the spectra of BSA both with and without the presence of AuNPs in this region, information about the different types of secondary structures such as α-helix, β-sheets, turns and random coil can be obtained. The spectrum of BSA in PBS displayed a strong signal between 1600 and 1700 cm^{-1}, while the spectrum of BSA and AuNPs in PBS showed changes in the strength and position of the absorption peak (Figure 3). This suggests that by interacting

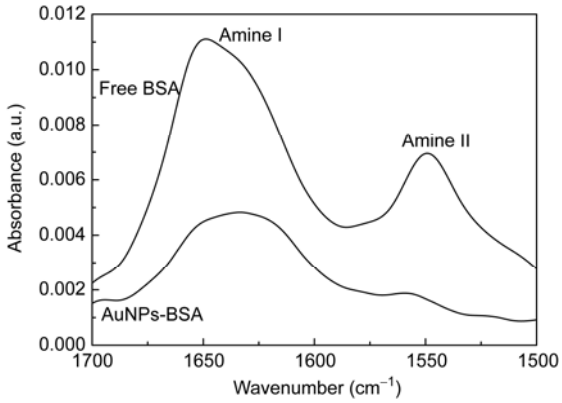

Figure 3 ATR-FTIR spectra of native BSA and BSA conjugated with AuNPs at pH 7.2 (after smoothing).

with AuNPs, changes in the secondary structures of BSA have occurred.

The second derivative of the region between 1600 and 1700 cm^{-1} and Fourier self-deconvolution were used to study these changes in detail. The frequencies of the component bands identified in the resolution enhanced spectrum were subsequently used as the input parameters for curve fitting of the original broad amide I band. Finally, with use of the Gaussian/Lorentzian profile, each spectrum was deconvoluted into seven peaks in the 1700–1600 cm^{-1} region (Figure 4). According to other protein-related research, the bands can be roughly assigned as follows [42–47]: 1660–1649 cm^{-1} (α-helix), 1638–1614 cm^{-1} (β-sheet), 1680–1660 cm^{-1} (β-turn), 1648–1640 cm^{-1} (random coil), and 1692–1680 cm^{-1} (antiparallel β sheet). Other reports suggested that the 1625 cm^{-1} band corresponds to the intramolecular β-strand structure, the 1616 cm^{-1} band is a result of intermolecular β-strand [48], and the 1610 cm^{-1} band is because of side-chain vibrations [49]. Therefore, the seven absorption bands in the BSA solution spectrum at 1693, 1669, 1653, 1648, 1637, 1626 and 1609 cm^{-1}, should correspond to antiparallel β sheet, β-turn, α-helix, random coil, β-sheet, intramolecular β-strand, and side-chain vibrations, respectively. After adding colloidal gold to BSA, new absorption bands were observed at 1699 cm^{-1} (antiparallel β sheet), 1671 cm^{-1} (β-turn), 1653 cm ^{1} (α-helix), 1648 cm^{-1} (random coil), 1637 cm^{-1} (β-sheet), and 1609 cm^{-1} (side-chain vibrations) in Figure 4. The appearance of the intermolecular β-strand band resulted from the unfolding of proteins, and the peak position changed from 1626 (intramolecular β-strand) to 1620 cm^{-1}. The total area of all the bands assigned to a given conformation were divided by the total area, and the number obtained was taken as the proportion of BSA in that conformation.

The curve-fitting results show that upon interaction with AuNPs, the α-helical content in BSA decreased from 41.5% to 25.3%, while the random coil content increased from 1.0% to 1.9%, β-sheet increased from 20.9% to 26.6%, and

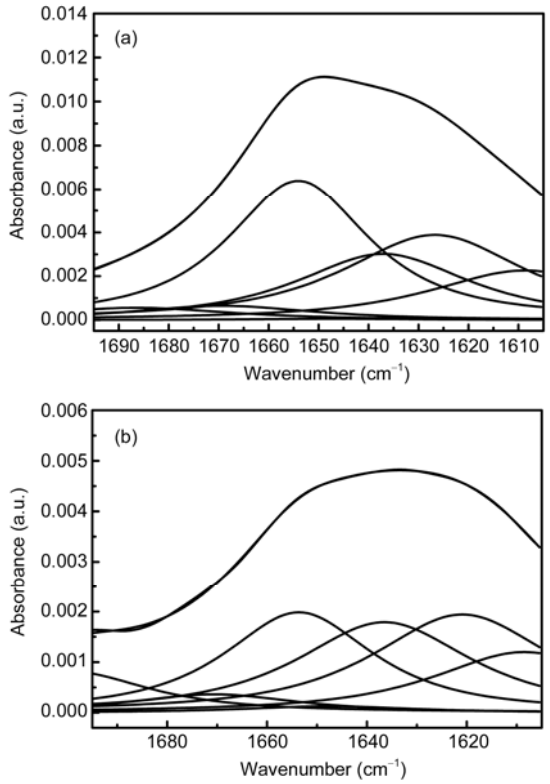

Figure 4 Curve fitting in the amide I region (1600–1700 cm^{-1}) with secondary structure determination of free BSA (a) and the AuNPs-BSA complex (b) in PBS (pH 7.2).

antiparallel β sheet increased from 4.2% to 11.1%. The reduction in the α-helix content in favor of the β-sheet, random coil, β-antiparallel and intermolecular β-strand structure is indicative of a partial unfolding of protein in the presence of the AuNPs. Compared to the conformation of BSA alone, these changes indicate the conformation of BSA in the presence of AgNPs become more flexible and more exposed to the solvent. It is possible that this conformational change resulted in the exposure of the hydrophobic cavities to more hydrophilic environments, and increased the polarity in the microenvironment around Trp-212 as discussed in Section 2.2. However, 61% of the α-helix, as compared with the BSA solution, was retained after the addition of AuNPs, probably because the high curvature of the AuNPs surface greatly favors the retention of the original structure of the protein. This is important for the application of the AuNPs-BSA bioconjugates in nanobiosensors, disease diagnostics, drug delivery, biological labeling and imaging, and where biological activity is required.

3 Conclusion

In this study, the interactions of BSA and AuNPs with a mean particle size of 13.9 nm were analyzed by UV-Vis, fluorescence and FTIR spectroscopic methods. It can be concluded that BSA adsorbs onto the surface of the AuNPs and acts to stabilize them in PBS. The critical adsorption density for preventing AuNP aggregation was 23 BSA molecules per gold particle or 3.8×10^{12} BSA molecules/cm^2. The fluorescence spectra showed that the AuNPs were a strong quencher and bound to BSA following the static quenching process with a high binding constant (K_s=7.59×10^8 L/mol). The number of binding sites indicates that there is on average one independent class of binding site on BSA for AuNPs. The formation of AuNPs-BSA conjugates led to a red shift in the intrinsic fluorescence emission of BSA. Both the data from fluorescence and ATR-FTIR analysis indicated that the tertiary and secondary structures of BSA were altered as it bound to the surface of the AuNPs, and these alterations forced the BSA structure to become less compact. This allowed the solvent to penetrate into the hydrophobic cavity of BSA and increase the polarity of the microenvironment around Trp-212.

This work was supported by the National Natural Science Foundation of China (*20974086*).

1 Daniel M C, Astruc D. Gold nanoparticles: Assembly, supramolecular chemistry, quantum-size-related properties, and applications toward biology, catalysis, and nanotechnology. Chem Rev, 2004, 104: 293–346
2 Niemeyer C M. Nanoparticles, proteins, and nucleic acids: Biotechnology meets materials science. Angew Chem Int Ed, 2001, 40: 4128–4158
3 Gole A, Dash C, Soman C, et al. On the preparation, characterization, and enzymatic activity of fungal protease-gold colloid bioconjugates. Bioconjugate Chem, 2001, 12: 684–690
4 Tkachenko A G, Xie H, Coleman D, et al. Multifunctional gold nanoparticle-peptide complexes for nuclear targeting. J Am Chem Soc, 2003, 125: 4700–4701
5 Keating C D, Kovaleski K M, Natan M J. Protein: Colloid conjugates for surface enhanced Raman scattering: Stability and control of protein orientation. J Phys Chem B, 1998, 102: 9404–9413
6 Lynch I, Dawson K A, Linse S. Detecting cryptic epitopes created by nanoparticles. Sci STKE, 2006, 2006: pe14
7 Fei L, Perrett S. Effect of nanoparticles on protein folding and fibrillogenesis. Int J Mol Sci, 2009, 10: 646–655
8 Dobrovolskaia M A, Patri A K, Zheng J, et al. Interaction of colloidal gold nanoparticles with human blood: Effects on particle size and analysis of plasma protein binding profiles. Nanomedicine, 2009, 5: 106–117
9 Lacerda S H D, Park J J, Meuse C, et al. Interaction of gold nanoparticles with common human blood proteins. ACS Nano, 2010, 4: 365–379
10 De R C, Courtoy P J, Baudhuin P. A model of protein-colloidal gold interactions. J Histochem Cytochem, 1987, 35: 1191–1198
11 Pramanik S, Banerjee P, Sarkar A, et al. Size-dependent interaction of gold nanoparticles with transport protein: A spectroscopic study. J Lumines, 2008, 128: 1969–1974
12 Teichroeb J H, Forrest J A, Jones L W. Size-dependent denaturing kinetics of bovine serum albumin adsorbed onto gold nanospheres. Eur Phys J E, 2008, 26: 411–415
13 Xie H, Tkachenko A G, Glomm W R, et al. Critical flocculation concentrations, binding isotherms, and ligand exchange properties of peptide-modified gold nanoparticles studied by UV-visible, fluorescence, and time-correlated single photon counting spectroscopies. Anal Chem, 2003, 75: 5797–5805
14 Jiang X, Jiang U G, Jin Y D, et al. Effect of colloidal gold size on the conformational changes of adsorbed cytochrome c: Probing by circu-

lar dichroism, UV-visible, and infrared spectroscopy. Biomacromolecules, 2005, 6: 46–53
15 Shang L, Wang Y Z, Jiang J G, et al. pH-dependent protein conformational changes in albumin: Gold nanoparticle bioconjugates: A spectroscopic study. Langmuir, 2007, 23: 2714–2721
16 Pan B, Cui D, Xu P, et al. Study on interaction between gold nanorod and bovine serum albumin. Colloid Surface A, 2007, 295: 217–222
17 Jans H, Liu X, Austin L, et al. Dynamic light scattering as a powerful tool for gold nanoparticle bioconjugation and biomolecular binding studies. Anal Chem, 2009, 81: 9425–9432
18 Wangoo N, Suri C R, Shekhawat G. Interaction of gold nanoparticles with protein: A spectroscopic study to monitor protein conformational changes. Appl Phys Lett, 2008, 92: 133104
19 Yang T, Li Z, Wang L, et al. Synthesis, characterization, and self-assembly of protein lysozyme monolayer-stabilized gold nanoparticles. Langmuir, 2007, 23: 10533–10538
20 Calzolai L, Franchini F, Gilliland D, et al. Protein-nanoparticle interaction: Identification of the ubiquitin-gold nanoparticle interaction site. Nano Lett, 2010, 10: 3101–3105
21 Iosin M, Toderas F, Baldeck P L, et al. Study of protein-gold nanoparticle conjugates by fluorescence and surface-enhanced Raman scattering. J Mol Struct, 2009, 924-926: 196–200
22 Sen T, Haldar K K, Patra A. Au nanoparticle-based surface energy transfer probe for conformational changes of BSA protein. J Phys Chem C, 2008, 112: 17945–17951
23 Jeyachandran Y L, Mielczarski E, Rai B, et al. Quantitative and qualitative evaluation of adsorption/desorption of bovine serum albumin on hydrophilic and hydrophobic surfaces. Langmuir, 2009, 25: 11614–11620
24 Burt J L, Gutierrez-Wing C, Miki-Yoshida M, et al. Noble-metal nanoparticles directly conjugated to globular proteins. Langmuir, 2004, 20: 11778–11783
25 Frens G. Controlled nucleation for the regulation of the particle size in monodisperse gold suspensions. Nat Phys Sci, 1973, 241: 20–22
26 Jiang Z L, Feng Z W, Li Y S, et al. Resonance scattering spectroscopic study of gold nanoparticle (in Chinese). Sci China Ser B-Chem, 2001, 31: 183–188
27 Storhoff J J, Elghanian R, Mucic R C, et al. One-pot colorimetric differentiation of polynucleotides with single base imperfections using gold nanoparticle probes. J Am Chem Soc, 1998, 120: 1959–1964
28 Yu H H, Jiang D S. Spectroscopic studies on electrostatically self-assembled gold nanoparticulate thin films. Spectrosc Spect Anal, 2002, 22: 511–514
29 Brewer S H, Glomm W R, Johnson M C, et al. Probing BSA binding to citrate-coated gold nanoparticles and surfaces. Langmuir, 2005, 21: 9303–9307
30 Gao D J, Tian Y, Bi S Y, et al. Studies on the interaction of colloidal gold and serum albumins by spectral methods. Spectrochim Acta Part A, 2005, 62: 1203–1208
31 Ojha B, Das G. The interaction of 5-(alkoxy)naphthalen-1-amine with bovine serum albumin and its effect on the conformation of protein. J Phys Chem B, 2010, 114: 3979–3986
32 Bourassa P, Kanakis C D, Tarantilis P, et al. Resveratrol, genistein, and curcumin bind bovine serum albumin. J Phys Chem B, 2010, 114: 3348–3354
33 Barreca D, Laganà G, Ficarra S, et al. Anti-aggregation properties of trehalose on heat-induced secondary structure and conformation changes of bovine serum albumin. Biophys Chem, 2010, 147: 146–152
34 Royer C A. Probing protein folding and conformational transitions with fluorescence. Chem Rev, 2006, 106: 1769–1784
35 Klajnert B, Stanislawska L, Bryszewska M, et al. Interactions between PAMAM dendrimers and bovine serum albumin. BBA-Proteins Proteomics, 2003, 1648: 115–126
36 Kang J, Liu Y, Xie M X, et al. Interactions of human serum albumin with chlorogenic acid and ferulic acid. BBA-Gen Subj, 2004, 1674: 205–214
37 Hu Y J, Liu Y, Zhao R M, et al. Spectroscopic studies on the interaction between methylene blue and bovine serum albumin. J Photochem Photobiol A, 2006, 179: 324–329
38 Naveenraj S, Anandan S, Kathiravan A, et al. The interaction of sonochemically synthesized gold nanoparticles with serum albumins. J Pharm Biomed Anal, 2010, 53: 804–810
39 Zhang Y Z, Dai J, Xiang X, et al. Studies on the interaction between benzidine and bovine serum albumin by spectroscopic methods. Mol Biol Rep, 2010, 37: 1541–1549
40 Bi S, Ding L, Tian Y, et al. Investigation of the interaction between flavonoids and human serum albumin. J Mol Struct, 2004, 703: 37–45
41 Cui Y, Wei Q Q, Park H K, et al. Nanowire nanosensors for highly sensitive and selective detection of biological and chemical species. Science, 2001, 293: 1289–1292
42 Surewicz W K, Mantsch H H, Chapman D. Determination of protein secondary structure by Fourier transform infrared spectroscopy: A critical assessment. Biochemistry, 1993, 32: 389–394
43 Zeng H T, Chittur K K, Lacefield W R. Analysis of bovine serum albumin adsorption on calcium phosphate and titanium surfaces. Biomaterials, 1999, 20: 377–384
44 Servagent-Noinville S, Revault M, Quiquampoix H, et al. Conformational changes of bovine serum albumin induced by adsorption on different clay surfaces: FTIR analysis. J Colloid Interface Sci, 2000, 221: 273–283
45 Hosseini-Nia T, Ismail A A, Kubow S. Effect of high hydrostatic pressure on the secondary structures of BSA and apo- and holo-alpha-lactalbumin employing Fourier transform infrared spectroscopy. J Food Sci, 2002, 67: 1341–1347
46 Charbonneau D M, Tajmir-Riahi H A. Study on the interaction of cationic lipids with bovine serum albumin. J Phys Chem B, 2010, 114: 1148–1155
47 Cheng H X, Liu H, Zhang Y Y, et al. Interaction of the docetaxel with human serum albumin using optical spectroscopy methods. J Lumines, 2009, 129: 1196–1203
48 Purcell M, Neault J F, Tajmir-Riahi H A. Interaction of taxol with human serum albumin. Biochim Biophys Acta, 2000, 1478: 61–68
49 Murayama K, Tomida M. Heat-induced secondary structure and conformation change of bovine serum albumin investigated by Fourier transform infrared spectroscopy. Biochemistry, 2004, 43: 11526–11532